International Symposium
On Turbulence and Shear Flow
Phenomena (TSFP-8)
August 28 - 30, 2013 Poitiers, France

STREAMWISE VARIATION OF TURBULENT DYNAMICS IN BOUNDARY LAYER FLOW WITH DRAG-REDUCING SURFACTANT INJECTION

Shinji Tamano
Graduate School of Engineering
Nagoya Institute of Technology
Gokiso-cho, Showa-ku, Nagoya, 466-8555, Japan
tamano.shinji@nitech.ac.jp

Takuya Kitao
Graduate School of Engineering
Nagoya Institute of Technology
Gokiso-cho, Showa-ku, Nagoya, 466-8555, Japan
cja16531@stn.nitech.ac.jp

Yohei Morinishi
Graduate School of Engineering
Nagoya Institute of Technology
Gokiso-cho, Showa-ku, Nagoya, 466-8555, Japan
morinishi.yohei@nitech.ac.jp

ABSTRACT

We investigated the difference in streamwise variations of turbulent dynamics between homogeneous and heterogeneous (injected) nonionic surfactant solutions using the flow visualization and two-component LDV and PIV measurements in drag-reducing turbulent boundary layer flows. It is found that streamwise variations in turbulence statistics for surfactant solution injection are similar with those of homogeneous surfactant solutions, except for the streamwise turbulence intensity and Reynolds shear stress.

INTRODUCTION

Surfactants are categorized into four types, namely, anionic, cationic, nonionic and zwitterionic. Among them, the cationic surfactant has been widely investigated as drag-reducing additives for wall-bounded turbulent flows, since it has high drag-reducing ability of up to 80% and is little affected by the degradation due to mechanical shear action (see e.g. Gyr and Bewersdorff, 1995; Zakin et al., 1998; Li et al., 2012). However, a cationic surfactant does not degrade naturally due to bacteria, so the potential damage to the environment is much higher than with nonionic surfactants. On the other hand, a nonionic surfactant is nontoxic and biodegradable, and the potential damage to the environment is much smaller than that of a cationic surfactant, although, until recent developments, the drag-reducing ability of nonionic surfactant was not so high.

In our recent work (Tamano et al., 2010), we investigated the drag-reducing effect of a nonionic surfactant on the turbulent boundary layer using two-component LDV and PIV systems. Turbulence statistics and structures for nonionic surfactant solutions showed the behavior of typical drag-reducing flow such as suppression of turbulence and modification of near-wall vortices, but they were different from those of drag-reducing cationic surfactant solutions (Tamano et al., 2009; 2011). It should be noted that nonionic and cationic surfactant aqueous solutions were homogeneous in our previous studies on the drag-reducing turbulent boundary layer flows (Itoh et al., 2005; Tamano et al., 2009; 2010; 2011).

On the other hand, Fontaine et al. (1992) and Hou et al. (2008) clarified the effects of polymer injection from the wall on the turbulent boundary layer using LDV and PIV systems, respectively. White and Mungal (2008) also found that the dependence of turbulence intensity of the velocity fluctuations on the drag reduction ratio was more complex compared to the turbulent channel flow (see e.g. Warholic et al., 1999; Li et al., 2006). However, the drag-reducing mechanism due to the injection of the nonionic surfactant aqueous solutions into turbulent boundary layer flows still remains unknown.

In this study, we conducted the flow visualization and two-component LDV and PIV measurements for a turbulent boundary layer with the drag-reducing nonionic surfactant injection from wall surface. We compared turbulence structures and turbulence statistics of injected (heterogeneous) nonionic surfactant solutions with those of homogenous nonionic surfactant solutions (Tamano et al., 2010).

EXPERIMENTAL APPARATUS AND PROCEDURE

Figure 1 shows the present experimental apparatus, which consists of the main part for the circulation of working fluids and the injection part of the surfactant solution. The closed-loop water tunnel with a cross section of 300 $\times$ 300 mm and a length of 1500 mm was used. A test plate of 20 $\times$ 295 $\times$ 1700 mm was installed in the water tunnel. All parts in contact with the surfactant solution were made of acrylic resin or stainless steel. A 1-mm diameter trip wire fixed at 100 mm downstream from the leading edge was used to develop the boundary layer on the test plate. Working fluids were circulated by a stainless steel centrifugal pump. The free-stream velocities U_e was set at about 300 mm/s. The injection slot located at $x = 300$ mm was

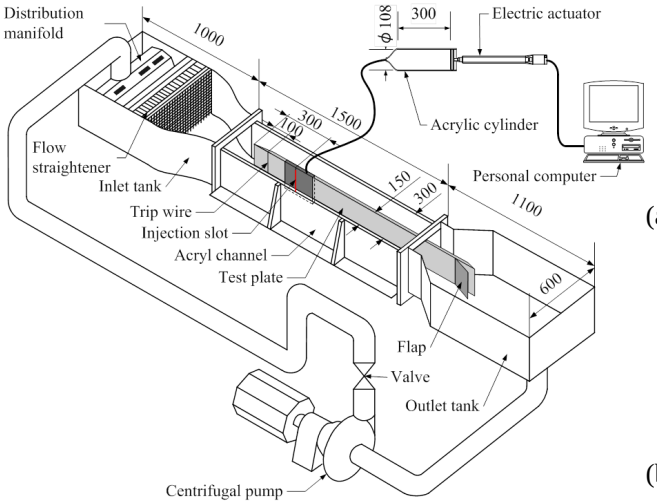

Figure 1. Experimental setup.

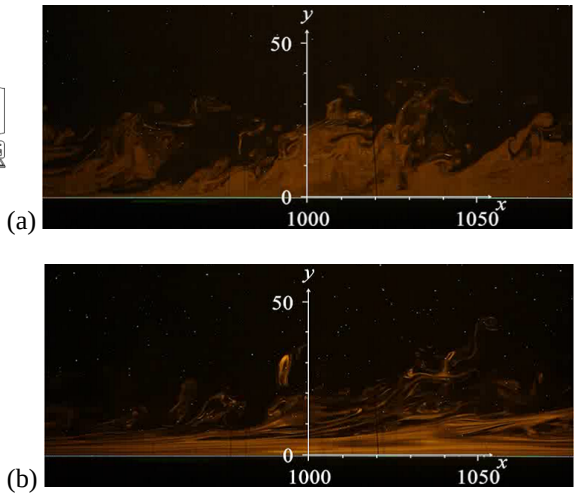

Figure 2. Flow visualization measurements around $x = 1000$ mm: (a) water injection, (b) ODMAO injection at $DR = 50\%$.

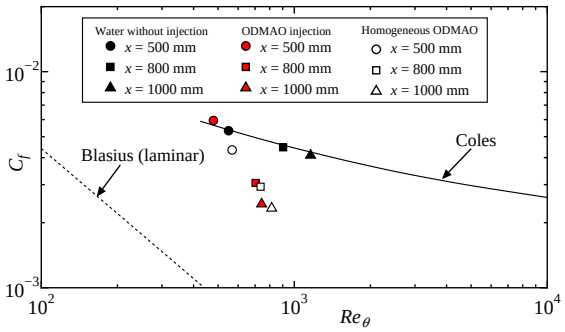

Figure 3. Friction coefficient versus Reynolds number.

inclined at 30° to the flat plate, which is determined by reference to Hou et al. (2008). The surfactant solution was injected into turbulent boundary layer through this injection slot with the PC control.

Regarding the flow visualization, the mixture of the visualization dye (Rhodamine B, 3 ppm) and the working fluid was injected into turbulent boundary layer. The streamwise and wall-normal ($x-y$) plane to the test plate was illuminated by the laser sheet (LYPE-2SG-WL532CW, output: 1.5 W, width: 2 mm, Japan Laser, Ltd.) through the side wall of the channel, and images were captured by a digital video camera (EOS 7D, Canon, Ltd.) from the bottom of the channel. The resolution was 5184×3456 pixels for images and 1920×1080 pixels for movies. The frame rate was set at 30 fps with a shutter speed of 1/2000 s.

Regarding the LDV measurement, the two-component LDV system with 300 mW argon-ion laser (Model 1895, Kanomax Japan, Inc.) was used in the back scatter mode. The flow was seeded with nylon powder particles (mean diameter: 4.1 μm; specific gravity: 1.02). LDV measurements were made 150 mm above the channel bottom. Data samples in the locations away from and near the wall are about 25000 and 10000, respectively.

Regarding the PIV measurement, the $x-y$ plane was illuminated by a laser sheet (DPSS Green Laser, output: 2 W, width: 1 mm, Japan Laser, Ltd.) through the side wall of the channel, and images were captured by a high-speed camera (FASTCAM-1024PCI, Photron, Ltd.). The high-speed camera had a resolution of 1024×1024 pixels. The frame rate was set at 1000 fps with a shutter speed of 1/5000 s. Flow was seeded with particles (Orgasol, mean diameter: 50 μm; specific gravity: 1.02). Turbulent statistics were obtained by evaluating about 52000 images in PIV vector fields. Fluctuating velocity vector fields were obtained by the Reynolds decomposition.

The flow visualization, LDV and PIV measurements were made 500, 800, and 1000 mm downstream of the leading edge. The temperature T of working fluids was 20°C, and the variation of T was controlled within ± 0.3°C during the measurements by two refrigerators.

The nonionic surfactant used here was AROMOX, which mainly consisted of oleyldimethylamineoxide (ODMAO), developed by Lion Akzo Co., Ltd., which was dissolved in tap water. The concentration of ODMAO was 500 ppm by weight. The shear viscosity of the surfactant solution was measured by a homemade capillary viscometer with an internal diameter of 5.0 mm (see Tamano et al., 2010 for details).

RESULTS AND DISCUSSIONS

Figure 2 shows the flow visualization results on $x-y$ plain around $x = 1000$ mm for water and nonionic surfactant (ODMAO) injections. Flow is from left to right. In the figure, $y = 0$ is the location of the wall. For the water injection, flow visualization dye displays very complex manner, which indicates the potential and turbulent flows are strongly mixed. On the other hand, for the surfactant injection, the flow visualization dye is almost parallel to the wall, which indicates that the layered structure is formed. The layered structure is a typical feature of drag-reducing flows with the large drag reduction ratio DR (the definition is explained later), as pointed out by Tamano et al. (2009; 2010; 2011). This also suggests that the wall-normal momentum transfer is strongly attenuated due to the surfactant injection.

Figure 3 shows the dependence of the friction coefficient $C_f = 2(u_\tau/U_e)^2$ on the momentum-thickness Reynolds number $Re_\theta = U_e\theta/\nu$, where u_τ and θ the friction velocity and momentum thickness, respectively. The

Table 1. Drag reduction ratio (DR [%]).

x [mm]	500	800	1000
Homogeneous ODMAO	18	40	50
ODMAO injection	−5	38	50

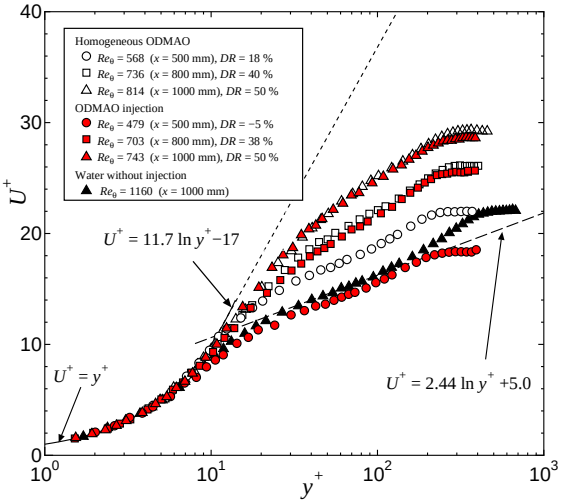

Figure 4. Mean velocity profiles.

solid and dashed lines represent Coles' curve (Coles, 1962) and Blasius laminar line, respectively. The data of C_f for water agree well with Coles' curve. The data of C_f versus the Reynolds number Re_θ are almost collapsed for surfactant injection and homogeneous surfactant solutions, in which the C_f drastically decreases with increasing Re_θ.

In the present study, the drag reduction ratio DR for the turbulent boundary layer is defined as follows:

$$DR = \frac{C_{f,\,\mathrm{water}} - C_{f,\,\mathrm{surfactant}}}{C_{f,\,\mathrm{water}}} \times 100, \qquad (1)$$

under the condition of the same momentum-thickness Reynolds number Re_θ. The C_f for water is obtained using the Coles' curve at the corresponding Reynolds number. The drag reduction ratios are presented in Table 1. It is noted that values of DR for both homogeneous and injection cases are the same at $x = 1000$ mm.

Figure 4 shows the profile of mean velocity in inner scaling $U^+ = U/u_\tau$. The dashed line shows the Newtonian log-law, and the dotted line represents the Virk log-law which is the Virk's ultimate profile (Virk, 1975), ($U^+ = 11.7 \ln y^+ - 17$) for polymer solutions, where $y^+ = u_\tau y/\nu$ is the distance from the wall scaled by the viscous length scale. It is seen that, with going downstream or with the increase in the amount of drag reduction, the mean velocity U^+ increases. A lot of previous experimental data support that the U^+ value increases with increasing the drag reduction ratio DR, which is independent of the homogeneous or heterogeneous surfactant solution. In the downstream region at $x = 800$ and 1000 mm, the mean velocities for surfactant injection agree well with those of homogeneous surfactant solutions at the corresponding streamwise locations.

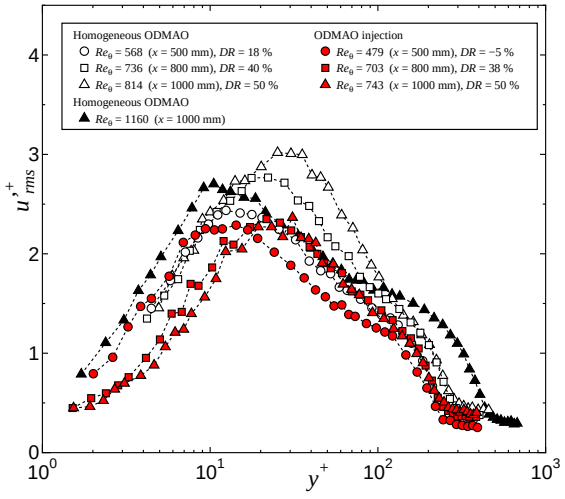

Figure 5. Profiles of streamwise turbulence intensity.

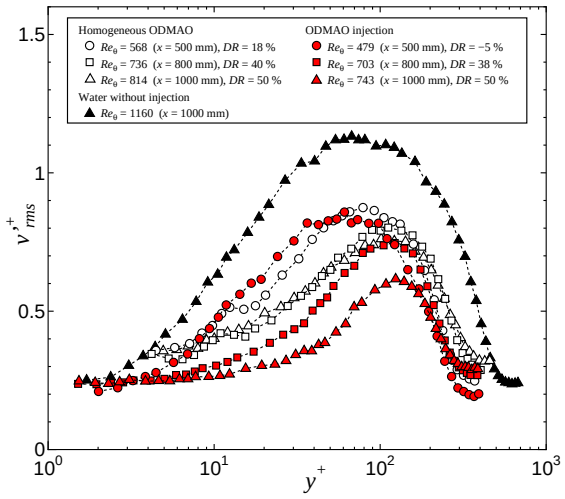

Figure 6. Profiles of wall-normal turbulence intensity.

Figure 5 shows distributions of streamwise turbulence intensity scaled by friction velocity u'^+_{rms}. For homogeneous surfactant solutions, the maximum of streamwise turbulence intensity increases in the streamwise direction. On the other hand, the maximum for the surfactant injection is almost constant. The maximum of the streamwise turbulence intensity for homogeneous surfactant solutions increases in the streamwise direction, while it is almost constant for surfactant injection. At this moment, the reason of this difference remains unknown, since the streamwise turbulence intensity is very sensitive to the Re_θ, DR, and how to develop the turbulent boundary layer. On the other hand, the locations of maximum of u'^+_{rms} monotonically increase with going downstream for both the surfactant injection and homogeneous surfactant solution.

Figure 6 shows distributions of wall-normal turbulence intensity v'^+_{rms}. For both the surfactant injection and homogeneous surfactant solution, the v'^+_{rms} gradually decreases in the streamwise direction, although the v'^+_{rms} for the homogeneous surfactant solution seems to be saturated at $x = 800$ mm. Unlike the behavior of maximum of the streamwise turbulence intensity, for both the cases, the maxima of wall-normal turbulence intensity decrease and the wall-normal

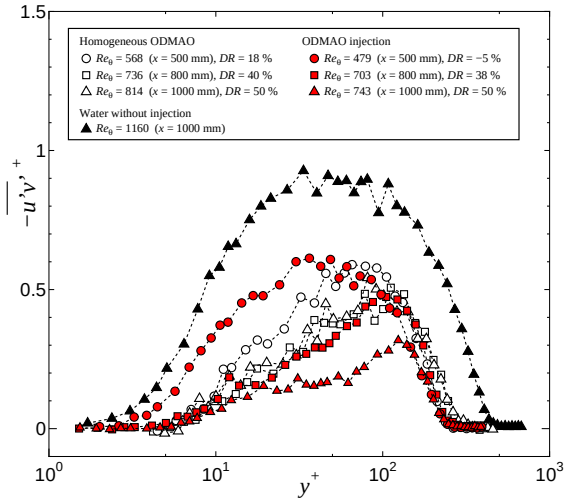

Figure 7. Profiles of Reynolds shear stress.

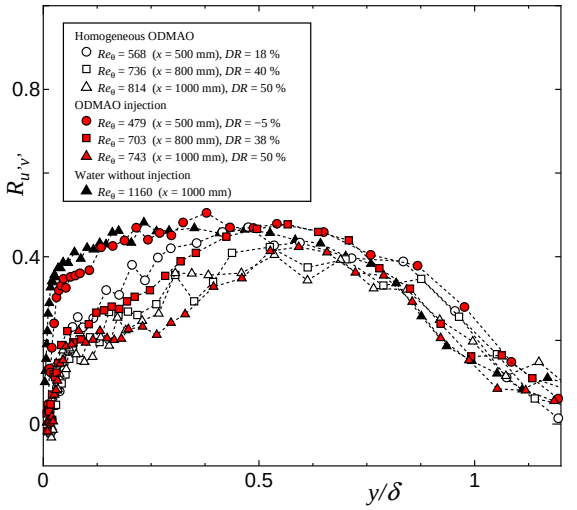

Figure 8. Profiles of correlation coefficient of streamwise and wall-normal turbulent fluctuations.

locations of maximum of v'^+_{rms} increase in the streamwise direction.

Figure 7 shows distributions of Reynolds shear stress $-\overline{u'v'}^+$. The Reynolds shear stresses for homogeneous and heterogeneous surfactant solutions at $x = 1000$ mm are much smaller than the corresponding water. For the homogeneous case, the profile of $-\overline{u'v'}^+$ at $x = 1000$ mm is almost the same as that at $x = 800$ mm, while for the injection case, the $-\overline{u'v'}^+$ at $x = 1000$ mm is smaller than that at $x = 800$ mm. For the case of ODMAO injection at $x = 1000$ mm ($DR = 50\%$), the plateau region is observed in the buffer region ($30 < y^+ < 70$).

Figure 8 shows distributions of the correlation coefficient of the streamwise and wall-normal turbulent fluctuations, $R_{u'v'} = -\overline{u'v'}/(u'_{rms}v'_{rms})$. The abscissae y/δ is the distance from the wall scaled by the boundary layer thickness δ. Except for the surfactant injection case at $x = 500$ mm, the $R_{u'v'}$ for both cases is smaller than that the corresponding water case at $y/\delta < 0.5$. The profiles of $R_{u'v'}$ at $x = 800$ and 1000 mm for the surfactant injection case are almost the same as those of the homogeneous case, unlike the Reynolds shear stress profiles.

Figures 9(a) and 9(b) show the time sequence realization of typical fluctuating velocity vector fields in $x-y$ plane for the water flow and the ODMAO injection at $DR =$ 50%. In the figure, $x'/\delta = 0$ corresponds to the location of $x = 1000$ mm. The vector represents the fluctuating velocity vector. For the water, we can observe several vortex cores (A to F), and some vortex cores seem to constitute hairpin vortex packets. For the ODMAO injection, on the other hand, the velocity fluctuations are attenuated across the turbulent boundary layer, and two vortex cores (G, H), the scale of which is larger than that of water, are observed. The fluctuating velocity vectors near the wall are almost parallel to the wall, which is consistent with the flow visualization [Fig. 2(b)] and almost the same as those of the homogeneous ODMAO surfactant solutions at the corresponding streamwise location (see Tamano et al., 2010).

CONCLUSIONS

We performed the flow visualization and two-component LDV and PIV measurements of drag-reducing turbulent boundary layer flows in order to clarify the difference in streamwise variations of turbulent dynamics between homogeneous and heterogeneous (injected) nonionic (ODMAO) surfactant solutions. The main results of the present study may be summarized as follows.

(1) Streamwise variations in boundary layer parameters, the friction coefficient, and mean velocity of surfactant solution injection are similar with those of homogeneous surfactant solutions.

(2) The maximum of streamwise turbulence intensity with the surfactant injection does not vary in the streamwise direction, while it increases in homogeneous surfactant solutions. The wall-normal locations of streamwise turbulence intensity are away from the wall with going downstream for both homogeneous and injection cases.

(3) The maximum of wall-normal turbulence intensity decreases in the streamwise direction, and the wall-normal location is away from the wall for both homogeneous and heterogeneous surfactant solutions.

(4) The Reynolds shear stresses for both homogeneous and heterogeneous surfactant solutions at $x = 1000$ mm are much smaller than the corresponding water. For the case of surfactant injection at $x = 1000$ mm ($DR = 50\%$), the plateau region is observed in the buffer region ($30 < y^+ < 70$).

(5) The profile of the correlation coefficient of the streamwise and wall-normal turbulent fluctuations at $x = 1000$ mm for the surfactant injection case is almost the same as that of the homogeneous case, unlike the Reynolds shear stress.

(6) The velocity fluctuations for the surfactant injection at $DR = 50\%$ are attenuated across the turbulent boundary layer, the scale of vortex cores is larger than that of water, and the fluctuating velocity vectors near the wall are almost parallel to the wall. Such observation is almost the same as that of the homogeneous nonionic surfactant solutions.

ACKNOWLEDGMENTS

It was supported by a Grant-in-Aid for Scientific Research (No. 23686029) from the Japan Society for the Promotion of Science. We are grateful to Mr. Y. Matsuno, Mr. N. Nakata, Mr. J. Ito, and Mr. K. Nishio for the assistance with the experimental measurements.

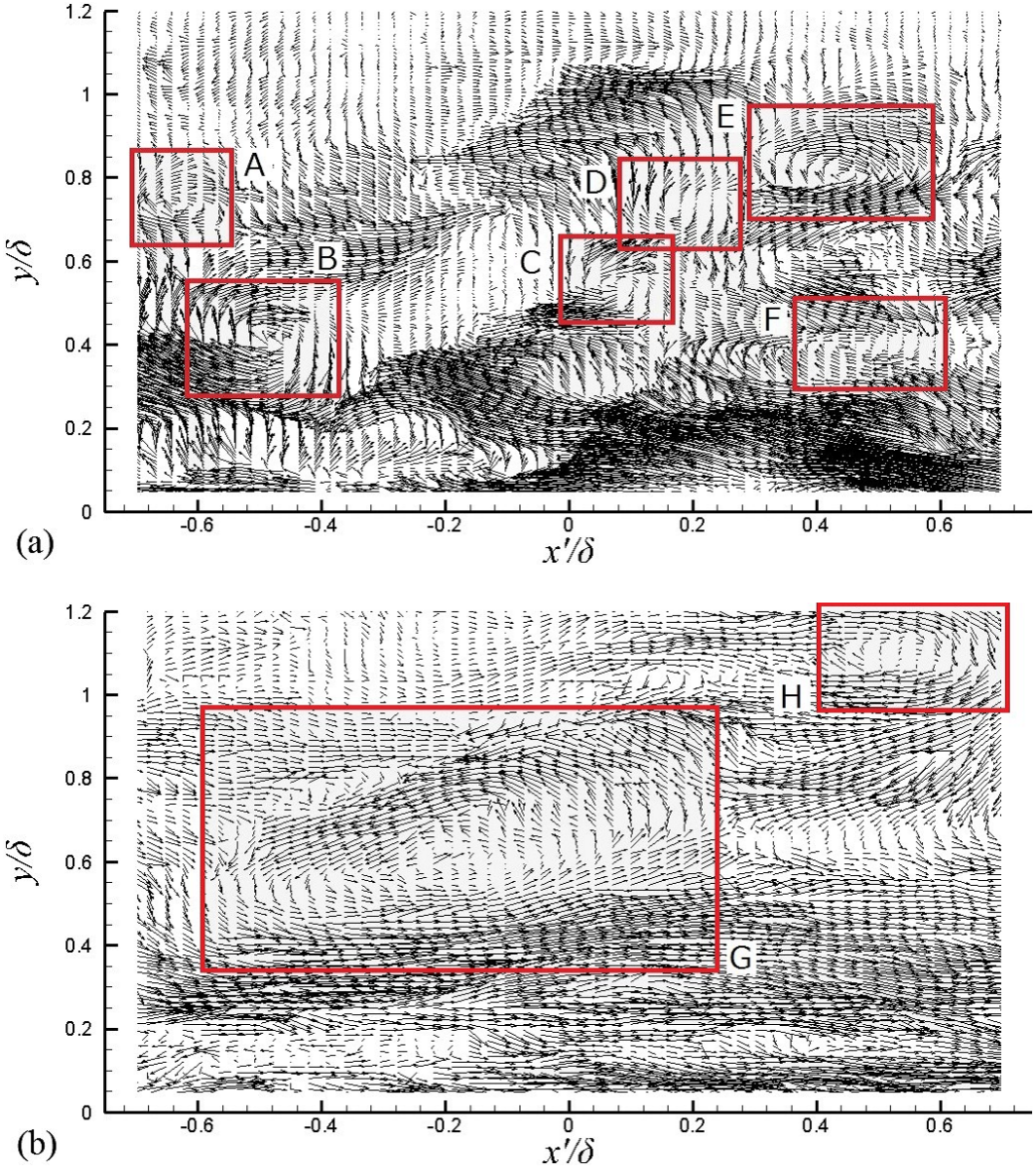

Figure 9. PIV measurements around $x = 1000$ mm: (a) water without injection, (b) ODMAO injection at $DR = 50\%$.

REFERENCES

Coles, D. E., 1962, "A manual of experimental boundary-layer practice for low-speed flow", *RAND Report*, No. R-403-PR.

Fontaine, A. A., Petrie, H. L., and Brungart, T. A., 1992, "Velocity profile statistics in turbulent boundary layer with slot-injected polymer", *Journal of Fluid Mechanics*, Vol. 238, pp. 435-466.

Gyr, A., and Bewersdorff, H.-W., 1995, *Drag reduction of turbulent flows by additives*, Kluwer Academic, Dordrecht, The Netherlands.

Hou, Y., Somandepalli, V. S. R., and Mungal, M. G., 2008, "Streamwise development of turbulent boundary-layer drag reduction with polymer injection", *Journal of Fluid Mechanics*, Vol. 597, pp. 31-66.

Itoh, M., Tamano, S., Yokota, K., and Ninagawa, M., 2005, "Velocity measurement in turbulent boundary layer of drag-reducing surfactant solution", *Physics of Fluids*, Vol. 17, No. 075107, pp. 1-9.

Li, F.-C., Kawaguchi, Y., Hishida, K., and Oshima, M., 2006, "Investigation of turbulence structures in a drag-reduced turbulent channel flow with surfactant additive by stereoscopic particle image velocimetry", *Experiments in Fluids*, Vol. 40, pp. 218-230.

Li, F.-C., Yu, B., Wei, J.-J., and Kawaguchi, Y., 2012, *Turbulent drag reduction by surfactant additives*, Joh Wiley and Sons Singapore Pte. Ltd.

Tamano, S., and Itoh, M., 2011, "Comparison of turbulence structures at large and small drag reduction ratios in turbulent boundary layer of surfactant solutions", *Journal of Turbulence*, Vol. 12, pp. 1-22.

Tamano, S., Itoh, M., Inoue, T., Kato, K., and Yokota, K., 2009, "Turbulence statistics and structures of drag-reducing turbulent boundary layer in homogenous aqueous surfactant solutions", *Physics of Fluids*, Vol. 21, No. 045101, pp. 1-19.

Tamano, S., Itoh, M., Kato, K., and Yokota, K., 2010, "Turbulent drag reduction in nonionic surfactant solutions", *Physics of Fluids*, Vol. 22, No. 055102, pp. 1-12.

Virk, P. S., 1975, "Drag reduction fundamentals", *AIChE Journal*, Vol. 21, pp. 625-656.

Warholic, M. D., Schmidt, G. M., and Hanratty, T. J., 1999, "The influence of a drag-reducing surfactant on a turbulent velocity field", *Journal of Fluid Mechanics*, Vol. 388, pp. 1-20.

White, C. M. and Mungal, M. G., 2008, "Mechanics and prediction of turbulent drag reduction with polymer additives", *Annual Review of Fluid Mechanics*, Vol. 40, pp. 235-256.

Zakin, J. L., Lu B., and Bewersdorff, H.-W., 1998, "Surfactant drag reduction", *Reviews in Chemical Engineering*, Vol. 14, pp. 253-318.